View Article Online
DOI: 10.1039/C6TA10609A

Journal of Materials Chemistry A

ARTICLE

Morphology Inherence from Hollow MOF to Hollow Carbon Polyhedron in Preparing Carbon-Based Electrocatalysts

Received 00th January 20xx,
Accepted 00th January 20xx

DOI: 10.1039/x0xx00000x

www.rsc.org/

Yuchen Pei,†[ab] Zhiyuan Qi,†[ab] Xinle Li,[ab] Raghu V. Maligal-Ganesh,[ab] Tian-Wei Goh,[ab] Chaoxian Xiao,[a] and Wenyu Huang[ab]*

Hollow carbon nanostructures are emerging as advanced electrocatalysts for the oxygen reduction reaction (ORR) due to the effective usage of active sites and the reduced dependence on expensive noble metals. Conventional preparation of these hollow structures is achieved through templates (*e.g.* SiO_2, CdS, and Ni_3C), which serve to retain the void interior during carbonization, leading to an essential template-removal procedure using hazardous acid etchants. Herein, we demonstrate the direct carbonization of unique hollow zeolitic imidazolate frameworks (ZIFs) for the synthesis of hollow carbon polyhedrons (HCPs) with well-defined morphology. The hollow ZIF precedent behaves bi-functionally as a carbon source and a morphology directing agent. This method evidences the strong morphology inherence of the hollow ZIFs during the carbonization, advancing the significant simplicity and environmental friendliness of this synthesis strategy. As-prepared HCPs show uniform polyhedral morphology and large void interiors, which enables their superior ORR activity. Iron can be doped into the HCPs (Fe/HCPs), rendering the Fe/HCPs with enhanced ORR property ($E_{1/2}$=0.850 V) in comparison with that of HCPs. We highlight the efficient structural engineering to transform MOF precedents into advanced carbon nanostructures accomplishing morphological control and high electrocatalytic activity.

Introduction

Hollow carbon nanostructures have gained considerable attention due to their high thermal stability, high surface-to-volume ratios, promoted usability of external active sites, and tunable compositions.[1-4] These advantages endow hollow carbon nanostructures with widespread applications as heterogeneous catalysts,[5] electrode materials,[6] and selective adsorbents for metal ions.[7] Of particular interest, carbon-based nanostructures are potential cathode materials to reduce the usage of expensive Pt catalysts for oxygen reduction reaction (ORR) in polymer-electrolyte-membrane fuel cells (PEMFCs).[8,9] The hollow carbon shells feature more easily accessible active sites due to the short diffusion length for reactants to access the active sites in the thin shells, and they also hold various capabilities for doping elements (*e.g.* Fe and N), which are beneficial to promote ORR activity.[8,10,11] The conventional synthesis of hollow carbon nanostructures usually starts from constructing a core/shell structure with sacrificial hard templates as core materials (*e.g.*, metal carbide,[6] quantum dots,[10] silica,[12] and polystyrene[13]) coated with carbon sources such as polymerized organic molecules. Subsequent pyrolysis can produce carbon sphere prototypes, where the subsequent removal of the core templates by the chemical etching is essential in most cases to afford the void interiors. Moreover, constrained by the morphology of sacrificial templates, the derived hollow carbon nanostructures are mostly spherical.[14] It is very challenging to prepare hollow carbon nanostructures with controlled morphologies in a more facile manner.[15-17]

Metal-organic framework (MOF) and MOF hybrids are an emerging class of crystalline porous materials with extensive applications.[18-27] Direct carbonization of MOF precedents has been exemplified as an ideal route to prepare porous carbon materials.[28-31] Benefitting from high surface areas, tunable functional groups, and controlled morphologies of the parent MOF precedents, MOF-derived porous carbons are also highly valued as active ORR catalysts.[32-38] Recently, considerable efforts have been devoted to developing hollow carbon nanostructures from the carbonization of MOF materials. Xu et al. obtained hollow carbon particles via the carbonization of Al-MIL-100 MOF, and subsequently removing the converged Al_2O_3 in the resultant carbonized materials by HF etching to induce void interiors.[39] Another interesting demonstration used a core/shell structure of zeolitic imidazolate framework (ZIF)/organic polymer hybrids, and the hollow interiors were generated *in situ* during carbonization.[40,41] Among these aforementioned strategies, the core/shell structure is essential

[a] Department of Chemistry, Iowa State University, Ames, Iowa 50011, United State.
[b] Ames Laboratory, U.S. Department of Energy, Ames, Iowa 50011, United States.
† These authors contribute equally.
* E-mail: whuang@iastate.edu
Electronic Supplementary Information (ESI) available.
See DOI: 10.1039/x0xx00000x

This journal is © The Royal Society of Chemistry 20xx

Please do not adjust margins

Published on 21 February 2017. Downloaded by Lawrence Berkeley National Laboratory on 21/02/2017 21:02:10.

Journal of Materials Chemistry A Accepted Manuscript

View Article Online
DOI: 10.1039/C6TA10609A

Published on 21 February 2017. Downloaded by Lawrence Berkeley National Laboratory on 21/02/2017 21:02:10.

in templates during carbonization to afford structural stability to the outer shell under high temperatures. We envisioned a direct transformation from hollow MOF precedents to hollow carbon particles, where the MOF shells can resist the structural collapse under the harsh carbonization conditions. This new strategy in preparing hollow carbons is inspired by the recent studies that MOF-derived carbons can inherit the morphology of their corresponding parent MOF precedents.[32,42] In comparison to previous core/shell template strategies, this hollow MOF to hollow carbon approach holds advantages including the easy operation, tunable composition, and completely avoiding hazardous etching chemicals (*e.g.* HF).

Herein, we present the preparation of well-defined hollow carbon polyhedrons (HCPs) by the direct carbonization of hollow ZIF precedents (Scheme 1). Hollow ZIF precedents behave bi-functionally as a carbon source and as a morphological template to construct HCPs. Remarkably, the prepared HCPs exhibited high ORR activity with a half-wave potential ($E_{1/2}$) of 0.821 V (vs. RHE) in basic conditions. We further doped Fe and 2,2'-bipyridine in the hollow MOF precedents. After carbonization, the Fe-doped HCPs exhibited 24% enhancement in current density compared to bare HCPs.

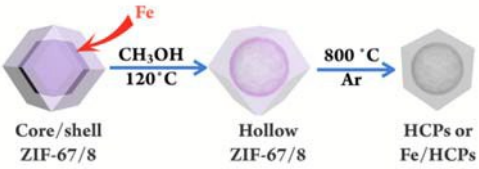

Scheme 1. The synthesis of HCPs from hollow ZIF-67/8 particles via a direct carbonization.

Experimental

Synthesis of hollow carbon polyhedrons (HCPs)

The synthesis method was carried out by following reported literature with modifications.[43] 0.546 g $Co(NO_3)_2{\cdot}6H_2O$, 0.558 g $Zn(NO_3)_2{\cdot}6H_2O$, and 0.616 g 2-methylimidazole were dissolve in respective 7.5, 7.5, and 15 mL methanol. Under sonication at 45 ˚C, the Co-methanol solution was added into 2-methylimidazole-methanol solution in 1 min, and the mixture was maintained under sonication for 5 min to form a purple suspension (ZIF-67 cores). The Zn-methanol solution was then added into the as-formed purple suspension in 2 min and sonicated for another 15 min. The suspension was then sealed into a solvothermal reactor and maintained at 120 ˚C for 2 h to form hollow ZIF-67/8 particles. Hollow ZIF-67/8 particles were centrifuged, washed, and dried in vacuum. The hollow ZIF-67/8 particles were carbonized to form HCPs in a quartz boat placed in a temperature-programmed tube furnace. The ramping rate was controlled at 1 ˚C/min, and the samples were carbonized at 800 ˚C for 3 h in a 50 mL/min flow of Ar.

Synthesis of Fe-doped hollow carbon polyhedrons (Fe/HCPs)

The synthesis and carbonization of Fe/HCPs are similar to HCPs, except for an extra Fe loading step before the coating of ZIF-8 shells in the preparation of core/shell ZIF-67/8 particles. As-formed ZIF-67 cores were centrifuged, washed, and dispersed in 15 mL methanol. After adding $Fe(NO_3)_3{\cdot}6H_2O$ and 2,2'-bipyridine, the mixture was stirred at room temperature for 24 h. The resulting Fe/ZIF-67 cores were centrifuged, washed and dispersed in 15 mL methanol solution containing 0.616g 2-methylimidazole. The Zn-methanol solution was then added to the mixture to form ZIF-8 shells. After methanol hydrothermal treatment and carbonization, Fe/HCPs were obtained.

Synthesis of solid carbon polyhedrons (SCPs)

SCPs were synthesized by similar procedures in preparing HCPs without the methanol hydrothermal treatment of the core-shell ZIF-67/8.

Characterization

N_2 physisorption experiments were conducted by using Micromeritics 3Flex surface characterization analyzer at 77 K. PXRD patterns of the samples were acquired by a STOE Stadi P powder diffractometer using Cu Kα radiation (40 kV, 40 mA, λ=0.1541 nm). Transmission electron microscopy (TEM) images were acquired by using a Tecnai G2 F20 electron microscope operated at 200 kV. ICP–MS (X Series II, Thermo Scientific) and ICP-OES (Perkin Elmer Optima 2100DV) were performed to determine the actual metal content. XPS spectra were measured by a PHI 5500 Multi-technique system (Physical Electronics, Chanhassen, MN) equipped with a mono-chromatized Al K_α X-ray source (1486.6 eV).

Electrochemical analysis of ORR

All electrochemical tests were measured using a potentiostat (VSP-300, Bio-Logic Science Instruments). Catalysts were dispersed in mixtures of H_2O:isopropanol:5% Nafion solution or isopropanol:H_2O:5% Nafion solution (4:1:0.025) to prepare a 2 mg/mL ink depending on the dispersion. After sonication for 30 min, 20 μL of the catalyst ink was applied onto a rotational ring-disk electrode (RRDE, 5 mm diameter) as a working electrode. A platinum wire and a saturated Ag/AgCl electrode were used respectively as the counter and the reference electrodes. The water used in all experiments was Millipore ultrapure water (18.2 mΩ). All ORR measurements were carried out at 25 ˚C in a 0.1 M KOH aqueous solution. The sweep speed for linear sweep voltammetry is 10 mV/s.

Results and Discussion

To fulfill the direct transformation from hollow MOF to hollow carbon nanostructure, hollow ZIF-67/8 particles were selected as the MOF precedent. ZIF-67 $[Co(MeIm)_2]_n$ (MeIm=2-methylimidazole) and ZIF-8 $[Zn(MeIm)_2]_n$ are isostructural MOF materials with similar zeolite SOD topology. Both of them consist of 2-methylimidazole linkers albeit with different metal sites (Co in ZIF-67 and Zn in ZIF-8). In general, ZIFs are optimum MOF precedents to achieve a high ORR activity of the resultant carbon materials due to the high nitrogen content in 2-methylimidazole linkers (ca. 30 wt.%). Moreover, the N atoms

Journal of Materials Chemistry A Accepted Manuscript

This journal is © The Royal Society of Chemistry 20xx

Please do not adjust margins

View Article Online
DOI: 10.1039/C6TA10609A

Published on 21 February 2017. Downloaded by Lawrence Berkeley National Laboratory on 21/02/2017 21:02:10.

are positioned within the aromatic ring, which increases the efficiency of N incorporation during carbonization.[29] The N species in (metal-doped) ZIF-derived carbon materials could also generate more metal-N species active in ORR, such as CoN_x and FeN_x.[32] In hollow ZIF-67/8-derived HCPs, the shorten diffusion length in the shell can facilitate the molecule transfer, beneficial to promote the ORR activity.[10]

Following this design principle, we first synthesized hollow ZIF-67/8 particles via a reported protocol,[43] and subsequently carbonized them to afford various carbon nanostructures. The hollow structure in ZIF-67/8 particles was employed by the selective destruction of ZIF-67 cores in core/shell ZIF-67/8 particles via the solvothermal route in methanol. The resultant hollow ZIF-67/8 particles show the well-defined rhombic dodecahedral morphology with deformed ZIF-67 fragments trapped inside. This synthesis is facile and does not require a hard template to sustain the hollow ZIF-67/8 precedents, and therefore precludes the laborious etching steps involved in removing internal templates after carbonization. Due to the morphology inherence during MOF carbonization,[32,42] we proposed that these hollow ZIF-67/8 particles could be directly carbonized to form HCPs, where the hollow nature of the ZIF-67/8 particles can be retained. It is notable that the retained ZIF-67 fragments readily restore a significant amount of Co in hollow ZIF-67/8 particles during the destruction of the ZIF-67 cores. This observation inspired us to utilize the ZIF-67 core as a carrier to dope other elements into the hollow ZIF-67/8 particles. Since Fe/N dopants in carbon materials can lead to enhanced ORR activities,[44,45] we loaded $Fe(NO_3)_3{\cdot}6H_2O$ and 2,2'-bipyridine as Fe and N precursors into ZIF-67 cores. The destruction of these Fe-doped ZIF-67 cores can induce Fe-doped hollow ZIF-67/8 particles, subsequently resulting in Fe-doped HCPs with enhanced ORR performance. In a nutshell, we anticipate that hollow ZIF-67/8 particles are ideal starting materials to prepare HCPs with superior ORR activity and controllable morphology.

Hollow ZIF-67/8 particles were first prepared with sizes ranging from 300 to 600 nm measured by TEM (Fig. 1a), of which the size and morphology are similar to their parent core/shell ZIF-67/8 precedents shown in Fig. 1b. They are endowed with large void interiors and a polyhedral morphology, which are advantageous in preparing HCPs. We observed the size enlargement of hollow ZIF-67/8 particles after methanol solvothermal treatment in comparison to their core/shell ZIF-67/8 counterparts as reported in literature.[43] With these hollow ZIF precedents, we proceeded to an elaborate carbonization to the hollow ZIF-67/8 particles at 800 ˚C for 3 h at a ramping rate of 1 ˚C/min in Ar atmosphere. As expected, as-synthesized HCPs (Fig. 1c) demonstrate well-defined polyhedral morphologies similar to their parent hollow ZIF-67/8 precedents. The hollow features of HCPs are clearly seen with the lighter interiors and their surrounding darker edges (Fig. 1e). The sizes of HCPs are similar to their hollow ZIF-67/8 precedents with a slight structural shrinkage. Several metal particles are also observed distributed across the HCPs' framework. These particles are presumed to be Co/CoO_x since only trace remnant of Zn was determined (<0.1 wt.%, Table S1) by inductively coupled plasma-mass spectrometry (ICP-MS) after the carbonization. To better evaluate the synthesis condition, we varied the carbonization temperatures (600, 800, and 1000 ˚C), time (1, 3, and 5 h at 800 ˚C) and atmosphere (Ar, N_2, and 10% H_2/Ar). Their ORR performances were shown in Figure S1 and Table S3. The carbonization condition of 3 h at 800 ˚C under Ar atmosphere is optimal to obtain the best ORR activity for HCPs. For the comparison, we also carbonized core/shell ZIF-67/8 particles to afford solid carbon polyhedrons (SCPs, as shown in Fig. 1d and f). Since the hollow ZIF-67/8 particles after methanol solvothermal treatment are larger than their core/shell ZIF-67/8 precursors,[43] the resultant HCPs is also larger than the as-prepared SCPs. Both HCPs and SCPs resembled their respective hollow and solid ZIF-67/8 precedents, which evidences the morphology inherence during MOF carbonization.

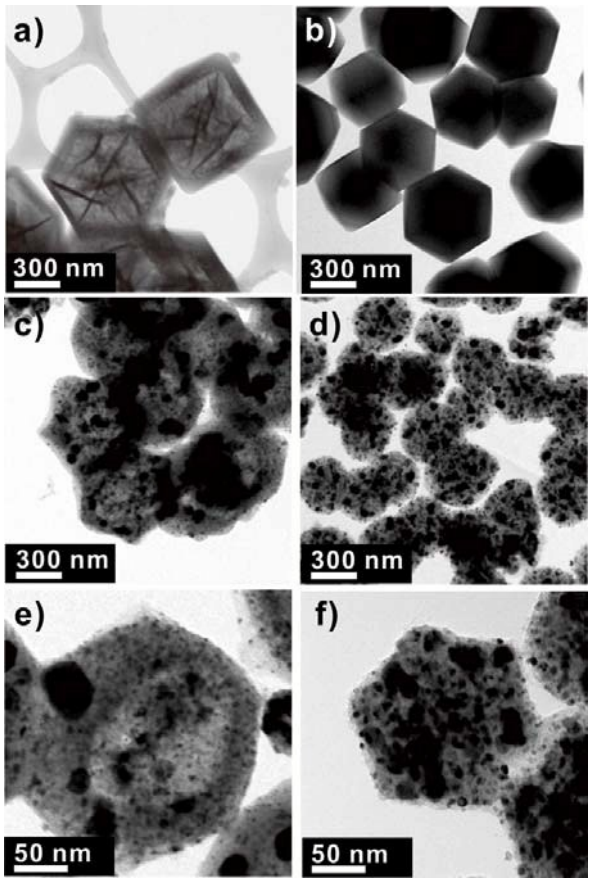

Fig. 1. TEM images of (a) hollow ZIF-67/8 particles, (b) core/shell ZIF-67/8 particles, (c) HCPs, and (d) SCPs. (e) and (f) are enlarged TEM images of respective HCPs and SCPs to identify the hollow interiors.

Co and Zn contents of HCPs, SCPs, and their parent ZIF-67/8 precedents were determined by ICP-MS (Table S1 in Supporting Information). Core/shell ZIF-67/8 particles consist of 18.2 wt.% Co and 5.5 wt.% Zn, conformed to the presence of both ZIF-67 cores and ZIF-8 shells. After methanol solvothermal treatment, hollow ZIF-67/8 particles show

Journal of Materials Chemistry A Accepted Manuscript

Please do not adjust margins

View Article Online
DOI: 10.1039/C6TA10609A

Published on 21 February 2017. Downloaded by Lawrence Berkeley National Laboratory on 21/02/2017 21:02:10.

increased Zn contents to 18.6 wt.%, presumably due to the mass reduction from the destruction of inner ZIF-67 cores. Co contents of hollow ZIF-67/8 particles decrease to 11.4 wt.%, indicating the significant retention of ZIF-67 fragments within the ZIF-8 shell. The carbonization of both hollow and core/shell ZIF-67/8 particles induces consistent weight loss of ca. 50 wt.%. The resultant HCPs and SCPs have Co contents of 23.9 and 41.3 wt.%, respectively. The roughly doubled Co contents in HCPs and SCPs, compared to that of their parent MOF precedents, are consistent with their weight losses. After the carbonization at 800 ˚C, less than 0.1 wt.% of Zn contents was detected in both HCPs and SCPs. The scarcity of Zn in HCPs and SCPs also confirms that the particles observed on the HCPs are Co/CoO_x nanoparticles in the TEM images. ICP-MS data of Co and Zn contents agree with the general carbonization pathway of ZIF-materials. 2-methylimidazole linkers pyrolyze into degraded hydrocarbons, whereas Co sites in ZIF-67 can form metallic Co and various carbides/nitrides species (CoN_x and CoC_x).[32] Under high temperatures, Zn can evaporate from the system due to their high vapor pressure, while Co species remain in the as-formed carbon materials.

We employed N_2 physisorption to characterize the porous structures of HCPs and SCPs as shown in Fig. 2a. The isotherms of both HCPs and SCPs show type IV characteristics. A distinct hysteresis loop of HCPs indicates more mesopore volume (0.47 $cm^3 \cdot g^{-1}$) in comparison to that of SCPs (0.35 $cm^3 \cdot g^{-1}$).[4,46,47] The pore size distributions of HCPs and SCPs agree with their mesoporous characters (Fig. 2b). The mesopores in SCPs are between 2-10 nm in diameter. Differing from SCPs, HCPs show a broader mesoporous feature centered at 60 nm corresponding to their void interiors. We noticed that the void space of 40-80 nm in size is smaller than the theoretical diameter (200-300 nm) of the hollow interior, assuming that HCPs could retain the morphology of their parent hollow ZIF-67/8 precedents. Contradictory to most intact hollow features of HCPs observed in TEM, we speculate that the size reduction of the hollow space shown in N_2-physisorption can be due to the presence of large metal nanoparticles or carbon structures that separate the void interior into several isolated compartments. Interestingly, the Brunauer-Emmett-Teller (BET) surface area of HCPs was measured as 227 $m^2 \cdot g^{-1}$, which is slightly lower than that of SCPs (282 $m^2 \cdot g^{-1}$). During the ZIF-67 core destruction to generate parent hollow ZIF-67/8 particles, degraded Co was reported to etch ZIF-8 shells.[43] Even though the void structure was retained after the carbonization of hollow ZIF-67/8 particles, we infer that the as-formed HCPs can undergo slight structural deformation under high temperatures. This deformation is due to the reduced thermal stability of the etched ZIF shell, which is also responsible for the observed lower BET surface areas in HCPs. The crystallization properties of HCPs, SCPs, and their parent ZIF-67/8 precedents were investigated by powder X-ray diffraction (PXRD) analysis (Fig. 3a). Both hollow and core/shell ZIF-67/8 particles exhibited well-crystallized ZIF structures. After carbonization, HCPs, and SCPs have similar PXRD patterns with amorphous structures. The broad feature around 25˚ is attributed to the (002) diffraction of graphitic carbon.[32] The series of distinct peaks at 22˚, 52˚, and 76˚ are characteristic peaks of bulk Co (PDF#15-0806), which reveals the presence of metallic Co nanoparticles in HCPs and SCPs.

Fe-doping and N-rich environment are critical to enhancing ORR activities of carbon materials.[10] We thus prepared the Fe-doped HCPs with similar hollow structures. As-prepared ZIF-67 cores were loaded with $Fe(NO_3)_3 \cdot 6H_2O$ as the Fe precursor and 2,2'-bipyridine as the additional N source. To accomplish the desirable hollow structure, ZIF-8 shells were then coated on the resulting Fe-loaded ZIF-67 cores to form the Fe-core/shell ZIF-67/8 particles. After methanol solvothermal treatment and carbonization, Fe-doped HCPs (denoted as Fe/HCPs) were obtained. The TEM images in Fig. 3b and S2 show that Fe/HCPs have similar morphological characteristics as bare HCPs. Target Fe/N loadings were controlled as 1.0 wt.% Fe and 2.0 wt.% 2,2'-bipyridine relative to the mass of ZIF-67 cores. The final Fe contents in Fe/HCPs were measured as 1.0 wt.% by inductively coupled plasma optical emission spectroscopy (ICP-OES). We further studied Co, Zn contents (Table S1) and PXRD features (Fig. S3) of Fe/HCPs, which agree well with that of HCPs.

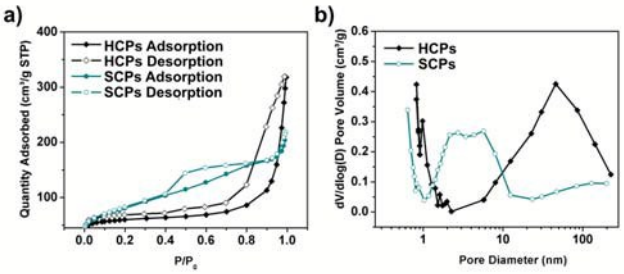

Fig. 2. (a) N_2 physisorption isotherms, and (b) pore size distributions of HCPs and SCPs.

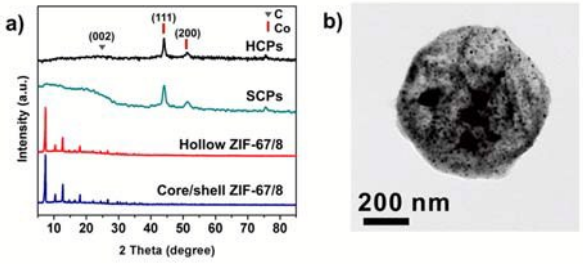

Fig. 3. (a) PXRD patterns of HCPs, SCPs, and their parent ZIF-67/8 precedents; (b) characteristic TEM images of Fe/HCPs.

Surface characteristics of HCPs, SCPs and Fe/HCPs were measured using X-ray photoelectron spectroscopy (XPS). Fig. S4 presents N 1s, Co 2p, Zn 2p, and Fe 2p spectra of respective carbon materials, and detailed analyses are summarized in Table S4. The HCPs have the highest surface N concentration at 6.7 at.% compared to SCPs (5.2 at.%) and Fe/HCPs (5.6 at.%). We deconvoluted the N peaks in XPS spectra to pyridinic-N, graphitic-N, and oxidized-N.[48,49] This indicates that most of the N atoms in the aromatic ring of 2-methyimidazole

Journal of Materials Chemistry A Accepted Manuscript

This journal is © The Royal Society of Chemistry 20xx

Please do not adjust margins

View Article Online
DOI: 10.1039/C6TA10609A

Published on 21 February 2017. Downloaded by Lawrence Berkeley National Laboratory on 21/02/2017 21:02:10.

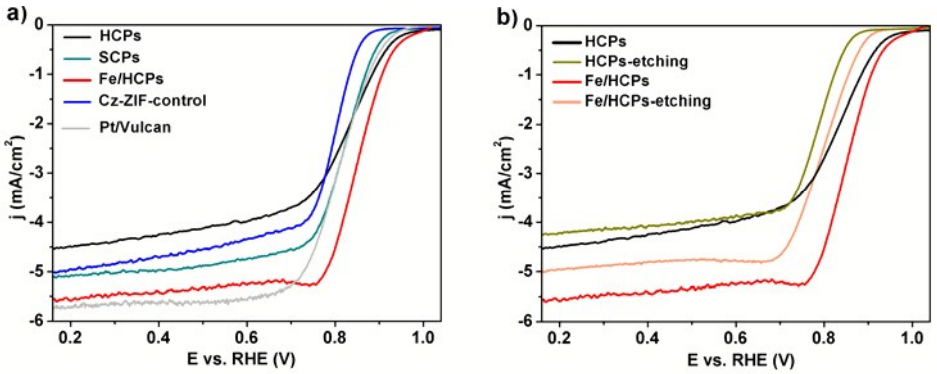

Fig. 4. (a) ORR polarization curves of HCPs, SCPs, Fe/HCPs, Cz-ZIF-control and commercial Pt/Vulcan catalysts. (b) ORR polarization curves of HCPs, HCPs-etching, Fe/HCPs, and Fe/HCPs-etching to investigate the active sites for ORR. In all ORR measurements, the ink concentrations of carbon catalysts and Pt/Vulcan were controlled as 2 mg/mL and 0.5 mg/mL. 20 µL of above mentioned catalyst ink was applied on the RRDE.

were transformed to these three types of N species.[33] HCPs and Fe/HCPs have consistently higher fractions of pyridinic-N and less oxidized-N compared to SCPs. The pyridinic-N species donate electrons to carbon networks, which is beneficial to ORR activity.[50] Co spectra depict that most of the Co surfaces are oxidized to CoO_x species. Consistent with low Zn contents in ICP-MS results, surface Zn is also observed to be less than 0.3 at.% in HCPs, SCPs and Fe/HCPs, confirming a nearly complete evaporation of Zn at high temperatures. Fe species were not detected on the surface of 1.0 wt.% Fe/HCPs. Since ICP-OES results confirm the presence of Fe in 1.0 wt.% Fe/HCPs, the low Fe contents in our samples may fall below the detection limit of XPS. Alternatively, Fe can be trapped inside the hollow structure of Fe/HCPs, where the Fe-doped ZIF-67 cores were used as the Fe carrier. This process can also be extended to dope other metal atoms into such hollow carbon structures.

With desired structural characterizations of HCPs and SCPs in place, we investigated their ORR activities using the rotating ring-disk electrode (RRDE) in a 0.1 M KOH electrolyte at 25 ˚C. Detailed potential and current density values are summarized in Table S5. As shown in Fig. 4, HCPs have an onset potential (E_{onset}) of 0.948 V, and $E_{1/2}$ is 0.821 V. To the best of our knowledge, these electrochemical values demonstrate our HCPs as highly active ORR catalysts comparing to previous reports (Table S6). Interestingly, SCPs have a comparable $E_{1/2}$ (0.810 V) and a lower E_{onset} (0.912 V) in contrast to that of the HCPs. However, the kinetic current density of HCPs (0.87 mA/cm² at 0.90 V) is ca. 2 times higher, in sharp contrast to that of SCPs (0.40 mA/cm²). It is interesting to note that the HCPs have lower surface area while demonstrating higher kinetic current density, which indicates that the hollow structure of HCPs can better utilize the easily accessible active sites accounting for ORR. To better evaluate the ORR activity of HCPs and SCPs, we prepared another carbonized bimetallic ZIF-67/8 as a control catalyst (denoted as Cz-ZIF-control) by co-mixing the Co/Zn precursors in the preparation of ZIFs. The Cz-ZIF-control shows solid structures with irregular shapes (Fig. S6).[34] We characterized Cz-ZIF-control using PXRD, XPS, ICP-MS, N_2 physisorption, and Raman spectrometry (Table S1-7 and Fig. S6-8). Solid Cz-ZIF-control displays mostly similar size, crystallization, and chemical properties in comparison to HCPs, except for the 30% lower surface N contents determined by XPS. We, therefore, tested ORR activity for this Cz-ZIF-control under identical conditions. Cz-ZIF-control has much worse ORR performance compared to HCPs. $E_{1/2}$ and E_{onset} of Cz-ZIF-control are 0.793 V and 0.869 V, which are 28 mV and 79 mV lower than HCPs. These electrochemical results demonstrate the synthesis and structural advantages of HCPs, which can promote their ORR activity.

It is notable that the limiting current of HCPs is 4.49 mA/cm² at 0.2 V, which is not competitive to Pt/Vulcan (5.73 mA/cm²) and SCPs (5.08 mA/cm²). We envision that the Fe-doping in Fe/HCPs can complement the low limiting current of HCPs due to the Fe promotion to ORR.[51] As expected, the current density of Fe/HCPs is boosted to 5.59 mA/cm², which is close to Pt/Vulcan and 24 % enhanced in comparison to that of HCPs. We also varied the Fe loadings from 0.4, 1.0, 3.3 and 19.8 wt.% on Fe/HCPs as determined by ICP-OES, and employed them for ORR analysis. 1.0 wt.% Fe ($E_{1/2}$ as 0.850 V) stands out as the most active catalysts among different Fe loadings under our synthesis and reaction conditions (Fig. S9 and Table S8), and this $E_{1/2}$ even surpasses that of HCPs by 29 mV. We propose that the Fe doping can facilitate the reduction of O_2 on the carbon surface responsible for the promotion of ORR current density in Fe/HCPs. To further validate this hypothesis, we placed HCPs and Fe/HCPs in 6 M HNO_3 overnight to etch the metallic contents, denoted as HCPs-etching and Fe/HCPs-etching (Table S1). After etching, Co contents are consistently reduced to ca. 30% for both HCPs and Fe/HCPs. The Fe content of Fe/HCPs-etching was measured as 0.9 wt.%, which is ca. 30% loss to that of the original Fe/HCPs considering the mass loss of Co. Fig. 4b illustrates the distinct decreasing ORR activity of both HCPs-etching and Fe/HCPs-etching in contrast to their respective counterparts before etching treatments. Respective $E_{1/2}$ of HCPs-etching (0.784 V) and Fe/HCP-etching (0.799 V) are similar, and they both contain comparable Co contents (ca. 8-12 wt.%). Limiting currents at 0.2 V of Fe/HCPs-etching (4.96 mA/cm²) are still 18% higher than HCPs-etching (4.22 mA/cm²), consistent with the adequate remnant Fe contents (ca. 70%) in Fe/HCPs-etching. We thus suggest that the Co

Journal of Materials Chemistry A Accepted Manuscript

Please do not adjust margins

View Article Online
DOI: 10.1039/C6TA10609A

Published on 21 February 2017. Downloaded by Lawrence Berkeley National Laboratory on 21/02/2017 21:02:10.

species on our HCPs and Fe/HCPs influence their ORR performance. Meanwhile, the doping of Fe can further increase the mass transport limiting current density, which evidences the promotion effect of Fe in ORR activity.[52-54] The chronoamperometric responses for HCPs and Fe/HCPs were also acquired for 40,000 s as shown in Fig. S10. Both HCPs and Fe/HCPs show excellent stabilities with respective 10.9 and 12.7% current drop, in comparison to the poor stability of Pt/Vulcan (53.0% current drop).

Conclusions

In summary, we demonstrate a novel and facile synthesis of hollow carbon polyhedrons (HCPs) via a direct carbonization of hollow ZIF-67/8 particles. This approach presents the morphology inherence of carbon materials derived from their parent MOF precedents. With the benefits afforded by the structural reassembly during carbonization, we designed the ideal Fe/HCPs catalyst with superior performance in ORR, combining the advantages of the high porosity of parent ZIFs, easily accessible active sites in hollow structures, and Fe-doping promotion. This work demonstrates the use of structural engineering for the preparation of porous carbon nanostructures in a controllable manner as efficient electrocatalysts.

Acknowledgements

We are grateful for the start-up funds support from the Ames Laboratory (Royalty Account) and Iowa State University. The Ames Laboratory is operated for the U.S. Department of Energy by Iowa State University under Contract No. DE-AC02-07CH11358. We thank Gordon J. Miller for the use of X-ray diffractometer, Igor I. Slowing for the use of ICP-OES, Xinwei Wang for the use of Raman spectrometer, and Dapeng Jing for the assistance in XPS measurements.

Notes and references

1 J. Liu, N. P. Wickramaratne, S. Z. Qiao and M. Jaroniec, *Nat. Mater.*, 2015, **14**, 763−774.
2 W. M. Zhang, J. S. Hu, Y. G. Guo, S. F. Zheng, L. S. Zhong, W. G. Song and L. J. Wan, *Adv. Mater.*, 2008, **20**, 1160−1165.
3 Q. Sun, W. C. Li and A. H. Lu, *Small*, 2013, **9**, 2086−2090.
4 X. Fang, J. Zang, X. Wang, M. S. Zheng and N. Zheng, *J. Mater. Chem. A*, 2014, **2**, 6191−6197.
5 R. Liu, S. M. Mahurin, C. Li, R. R. Unocic, J. C. Idrobo, H. Gao, S. J. Pennycook and S. Dai, *Angew. Chem. Int. Ed.*, 2011, **50**, 6799−6802.
6 Z. L. Schaefer, M. L. Gross, M. A. Hickner and R. E. Schaak, *Angew. Chem. Int. Ed.*, 2010, **49**, 7045-7048.
7 D. H. Liu, Y. Guo, L. H. Zhang, W. C. Li, T. Sun and A. H. Lu, *Small*, 2013, **9**, 3852−3857.
8 Y. Hu, J. O. Jensen, W. Zhang, L. N. Cleemann, W. Xing, N. J. Bjerrum and Q. Li, *Angew. Chem. Int. Ed.*, 2014, **53**, 3675−3679.
9 J. Sun, H. Yin, P. Liu, Y. Wang, X. Yao, Z. Tang and H. Zhao, *Chem. Sci.*, 2016, **7**, 5640-5646.
10 Y. Wang, A. Kong, X. Chen, Q. Lin and P. Feng, *ACS Catal.*, 2015, **5**, 3887−3893.
11 C. Han, S. Wang, J. Wang, M. Li, J. Deng, H. Li and Y. Wang, *Nano Res.*, 2014, **7**, 1809−1819.
12 N. Jayaprakash, J. Shen, S. S. Moganty, A. Corona and L. A. Archer, *Angew. Chem. Int. Ed.*, 2011, **50**, 5904−5908.
13 J. Han, G. Xu, B. Ding, J. Pan, H. Dou and D. R. MacFarlane, *J. Mater. Chem. A*, 2014, **2**, 5352−5357.
14 F. Caruso, R. A. Caruso and H. Möhwald, *Science*, 1998, **282**, 1111−1114.
15 W. Xia, J. Zhu, W. Guo, L. An, D. Xia and R. Zou, *J. Mater. Chem. A*, 2014, **2**, 11606−11613.
16 H. Wu, X. Qian, H. Zhu, S. Ma, G. Zhu and Y. Long, *RSC Adv.*, 2016, **6**, 6915−6920.
17 W. Li, X. Wu, H. Liu, J. Chen, W. Tang and Y. Chen, *New J. Chem.*, 2015, **39**, 7060−7065.
18 R. C. Huxford, J. Della Rocca and W. Lin, *Curr. Opin. Chem. Biol.*, 2010, **14**, 262−268.
19 L. E. Kreno, K. Leong, O. K. Farha, M. Allendorf, R. P. Van Duyne and J. T. Hupp, *Chem. Rev.*, 2011, **112**, 1105−1125.
20 S. Sen, N. N. Nair, T. Yamada, H. Kitagawa and P. K. Bharadwaj, *J. Am. Chem. Soc.*, 2012, **134**, 19432−19437.
21 J. A. Mason, M. Veenstra and J. R. Long, *Chem. Sci.*, 2014, **5**, 32−51.
22 X. Li, Z. Guo, C. Xiao, T. W. Goh, D. Tesfagaber and W. Huang, *ACS Catal.*, 2014, **4**, 3490−3497.
23 X. Li, T. W. G. Goh, C. Xiao, A. L. D. Stanton, Y. Pei, P. K. Jain and W. Huang, *ChemNanoMat*, 2016, **2**, 810−815.
24 H. Yin and Z. Tang, *Chem. Soc. Rev.*, 2016, **45**, 4873-4891.
25 L. He, Y. Liu, J. Liu, Y. Xiong, J. Zheng, Y. Liu and Z. Tang, *Angew. Chem. Int. Ed.*, 2013, **52**, 3741-3745.
26 S. Zhao, Y. Wang, J. Dong, C.-T. He, H. Yin, P. An, K. Zhao, X. Zhang, C. Gao, L. Zhang, J. Lv, J. Wang, J. Zhang, A. M. Khattak, N. A. Khan, Z. Wei, J. Zhang, S. Liu, H. Zhao and Z. Tang, *Nat. Energy*, 2016, **1**, 16184-16194.
27 W Cai, T. Lee, M. Lee, W. Cho, D. Y. Han, N. Choi, A. C. Yip and J. Choi, *J. Am. Chem. Soc.*, 2014, **136**, 7961-7971.
28 B. Liu, H. Shioyama, T. Akita and Q. Xu, *J. Am. Chem. Soc.*, 2008, **130**, 5390−5391.
29 W. Xia, A. Mahmood, R. Zou and Q. Xu, *Energy Environ. Sci.*, 2015, **8**, 1837−1866.
30 S. J. Yang, T. Kim, J. H. Im, Y. S. Kim, K. Lee, H. Jung and C. R. Park, *Chem. Mater.*, 2012, **24**, 464−470.
31 X.-W. Liu, T.-J. Sun, J.-L. Hu and S.-D. Wang, *J. Mater. Chem. A*, 2016, **4**, 3584-3616.
32 Y. Z. Chen, C. Wang, Z. Y. Wu, Y. Xiong, Q. Xu, S. H. Yu and H. L. Jiang, *Adv. Mater.*, 2015, **27**, 5010−5016.
33 J. Tang, R. R. Salunkhe, J. Liu, N. L. Torad, M. Imura, S. Furukawa and Y. Yamauchi, *J. Am. Chem. Soc.*, 2015, **137**, 1572−1580.
34 A. Aijaz, J. Masa, C. Rosler, W. Xia, P. Weide, A. J. Botz, R. A. Fischer, W. Schuhmann and M. Muhler, *Angew. Chem. Int. Ed.*, 2016, **55**, 4087−4091.
35 A. Aijaz, N. Fujiwara and Q. Xu, *J. Am. Chem. Soc.*, 2014, **136**, 6790−6793.
36 S. Zhao, H. Yin, L. Du, L. He, K. Zhao, L. Chang, G. Yin, H. Zhao, S. Liu and Z. Tang, *ACS Nano*, 2014, **8**, 12660-12668.
37 K. Shen, X. Chen, J. Chen and Y. Li, *ACS Catal.*, 2016, **6**, 5887-5903.
38 M. Li, W. Wang, M. Yang, F. Lv, L. Cao, Y. Tang, R. Sun and Z. Lu, *RSC Adv.*, 2015, **5**, 7356-7362
39 A. Aijaz, J. K. Sun, P. Pachfule, T. Uchida and Q. Xu, *Chem. Commun.*, 2015, **51**, 13945−13948.
40 S. Hong, J. Yoo, N. Park, S. M. Lee, J. G. Park, J. H. Park and S. U. Son, *Chem. Commun.*, 2015, **51**, 17724−17727.
41 S. Yang, L. Peng, P. Huang, X. Wang, Y. Sun, C. Cao and W. Song, *Angew. Chem. Int. Ed.*, 2016, **55**, 4016−4020.

Journal of Materials Chemistry A Accepted Manuscript

This journal is © The Royal Society of Chemistry 20xx

Please do not adjust margins

View Article Online
DOI: 10.1039/C6TA10609A

42 G. Srinivas, V. Krungleviciute, Z. X. Guo and T. Yildirim, *Energy Environ. Sci*., 2014, **7**, 335−342.
43 J. Yang, F. Zhang, H. Lu, X. Hong, H. Jiang, Y. Wu and Y. Li, *Angew. Chem. Int. Ed.*, 2015, **54**, 10889−10893.
44 J. Tian, A. Morozan, M. T. Sougrati, M. Lefevre, R. Chenitz, J. P. Dodelet, D. Jones and F. Jaouen, *Angew. Chem. Int. Ed.*, 2013, **52**, 6867−6870.
45 E. Proietti, F. Jaouen, M. Lefèvre, N. Larouche, J. Tian, J. Herranz and J. P. Dodelet, *Nat. Commun.*, 2011, **2**, 416-424.
46 T. Yang, J. Liu, R. Zhou, Z. Chen, H. Xu, S. Z. Qiao and M. J. Monteiro, *J. Mater. Chem. A*, 2014, **2**, 18139−18146.
47 S. Chen, J. Bi, Y. Zhao, L. Yang, C. Zhang, Y. Ma, Q. Wu, X. Wang and Z. Hu, *Adv. Mater.*, 2012, **24**, 5593−5597.
48 T. S. Olson, S. Pylypenko and P. Atanassov, *J. Phys. Chem. C*, 2010, **114**, 5049−5059.
49 V. B. Parambhath, R. Nagar and S. Ramaprabhu, *Langmuir*, 2012, **28**, 7826−7833.
50 S. Yasuda, L. Yu, J. Kim and K. Murakoshi, *Chem. Commun.*, 2013, **49**, 9627−9629.
51 Q. Yi, Y. Zhang, X. Liu, B. Xiang and Y. Yang, *J. Mater. Sci.*, 2014, **49**, 729−736.
52 J. S. Lee, G. S. Park, S. T. Kim, M. Liu and J. Cho, *Angew. Chem.*, 2013, **125**, 1060−1064.
53 H. Liu, M. Dou, F. Wang, J. Liu, J. Ji and Z. Li, *RSC Adv.*, 2015, **5**, 66471−66475.
54 Z. Y. Yang, Y. X. Zhang, L. Jing, Y. F. Zhao, Y. M. Yan and K. N. Sun, *J. Mater. Chem. A*, 2014, **2**, 2623−2627.

Published on 21 February 2017. Downloaded by Lawrence Berkeley National Laboratory on 21/02/2017 21:02:10.

Journal of Materials Chemistry A Accepted Manuscript

Please do not adjust margins

View Article Online
DOI: 10.1039/C6TA10609A

Published on 21 February 2017. Downloaded by Lawrence Berkeley National Laboratory on 21/02/2017 21:02:10.

Table of contents

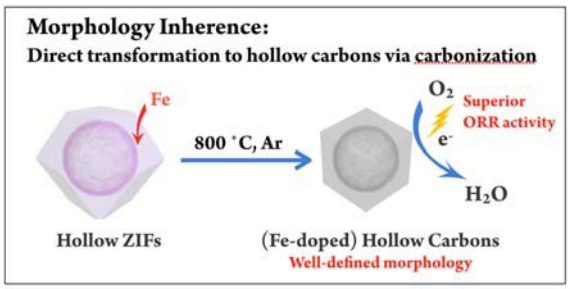

Direct transformation of hollow ZIFs to well-defined (Fe-doped) HCPs with superior ORR activities, benefiting from the morphology inherence during carbonization.

Journal of Materials Chemistry A Accepted Manuscript

View publication stats